

# On the Common Envelope Efficiency

Zhao-Yu Zuo<sup>1,3\*</sup> and Xiang-Dong Li<sup>2,3</sup>

<sup>1</sup>*Department of Physics, School of Science, Xi'an Jiaotong University, Xi'an 710049, China*

<sup>2</sup>*Department of Astronomy, Nanjing University, Nanjing 210093, China*

<sup>3</sup>*Key laboratory of Modern Astronomy and Astrophysics (Nanjing University), Ministry of Education, Nanjing 210093, China*

20 May 2014

## ABSTRACT

In this work, we try to use the apparent luminosity versus displacement (i.e.,  $L_X$  vs.  $R$ ) correlation of high mass X-ray binaries (HMXBs) to constrain the common envelope (CE) efficiency  $\alpha_{CE}$ , which is a key parameter affecting the evolution of the binary orbit during the CE phase. The major updates that crucial for the CE evolution include a variable  $\lambda$  parameter and a new CE criterion for Hertzsprung gap donor stars, both of which are recently developed. We find that, within the framework of the standard energy formula for CE and core definition at mass  $X = 10\%$ , a high value of  $\alpha_{CE}$ , i.e., around 0.8-1.0, is more preferable, while  $\alpha_{CE} < \sim 0.4$  likely can not reconstruct the observed  $L_X$  vs.  $R$  distribution. However due to an ambiguous definition for the core boundary in the literature, the used  $\lambda$  here still carries almost two order of magnitude uncertainty, which may translate directly to the expected value of  $\alpha_{CE}$ . We present the detailed components of current HMXBs and their spatial offsets from star clusters, which may be further testified by future observations of HMXB populations in nearby star-forming galaxies.

**Key words:** binaries: close — galaxies: star-burst — stars: evolution — X-ray: binaries — stars: distribution

## 1 INTRODUCTION

One of the most important stages in the evolution of close binary stars is common envelope (CE) evolution. It is commonly thought to occur when the expanding primary star transfers mass to its companion at a too high rate that the companion cannot accrete it. This leads to the companion star being engulfed by the envelope of the primary. The orbital energy and angular momentum of the orbiting components are then transferred into the CE, resulting in the orbital decay and spiral-in of the star (for a recent review, see Ivanova et al. 2013, and references therein). Two main schemes have been developed to describe the CE process. One (and the most popular one) is  $\alpha_{CE}$ -formalism (Webbink 1984). Usually the parameter  $\alpha_{CE}$  (see Eq 2 in this paper) in this scheme is introduced, to describe the efficiency of converting the orbital energy into the kinetic energy of the envelope, resulting in the ejection of the envelope. If there is sufficient energy ( $\propto \alpha_{CE}$ ) that can be used to eject the envelope, the system will survive to be a compact binary, otherwise the two stars coalesce instead. The other is the so-called  $\gamma$ -algorithm,

which considers angular momentum transformation during the spiral-in (Nelemans et al. 2000; Nelemans & Tout 2005). Despite extensive three dimensional hydrodynamical simulations (e.g., Rasio & Livio 1996; Sandquist et al. 1998, 2000; Fryxell et al. 2000; O'Shea et al. 2005; Fryer et al. 2006; Passy et al. 2012; Ricker & Taam 2012), the physics of the CE evolution still remains poorly understood.

Many efforts have been made to constrain the value of  $\alpha_{CE}$ . An important way is to use individual post-common-envelope binaries (PCEBs) to derive the magnitude of  $\alpha_{CE}$  (Maxted et al. 2006). Two recent works in this respect were made by Zorotovic et al. (2010) and De Marco et al. (2011), independently based on the Sloan Digital Sky Survey (SDSS) data of white dwarf/main-sequence (WDMS) binaries. By reconstructing the evolution of WDMS binaries, they can derive the value of  $\alpha_{CE}$ , i.e., around 0.2 – 0.3. An important progress in their studies is that they used a more realistic approximation for the envelope binding energy (i.e., parameter  $\lambda$ , see Eq 2) than a constant one. Their results also imply that future binary population synthesis (BPS) simulations with a proper treatment of  $\lambda$  is necessary and required urgently. An alternative way to constrain  $\alpha_{CE}$  is to perform BPS simulations. By comparing the predictions with the observed properties of PCEBs, the value of

\* E-mail: zuozyu@gmail.com

$\alpha_{\text{CE}}$  could be properly constrained. A lot of works have been carried out in this direction over the past two decades. The research targets cover a large variety of different PCEB populations, including WDMS (Politano & Weiler 2006, 2007; Davis et al. 2010, and see references therein), extreme horizontal branch stars (Han et al. 2002, 2003; Han 2008), low-mass X-ray binaries (Podsiadlowski et al. 2003), and high-mass X-ray binaries (HMXBs, Zuo & Li 2010, 2014b), etc. However most of the previous BPS studies adopted a rather simplified treatment of  $\lambda$ , as a constant, around 0.5 typically. It is worth noting that among the studies mentioned above, Davis et al. (2010) and Zuo & Li (2014b) have used a more realistic treatment of  $\lambda$  in their simulations. For example, Zuo & Li (2014b), by incorporating variable values of  $\lambda$  into the BPS code, constrained the CE mechanisms based on the measured X-ray luminosity function of HMXBs, and found that the  $\alpha_{\text{CE}}$ -formalism is more preferable and the value of  $\alpha_{\text{CE}}$  is likely high, i.e.  $\sim 0.5 - 1$ .

Note that, in our previous work (Zuo & Li 2010), indications already revealed that the X-ray luminosity versus displacement (i.e.,  $L_X$  vs.  $R$ ) distribution of HMXBs from star clusters in star-forming galaxies may provide a clue to constrain the value of  $\alpha_{\text{CE}}$ . Based on data from *Chandra* and NICMOS on board *Hubble Space Telescope (HST)* of X-ray sources and star clusters, respectively, Kaaret et al. (2004) found that the X-ray sources are generally located near the star clusters, and the brighter ones are preferentially closer to the clusters. Moreover there is an absence of luminous sources ( $L_X > 10^{38} \text{ erg s}^{-1}$ ) at relatively large displacements ( $> 200 \text{ pc}$ ) from the clusters. Based on this, we have modeled the kinematic evolution of XRBs from the star clusters from a theoretical point of view. It is shown that the parameter  $\alpha_{\text{CE}}$ , by affecting the binary orbit during the CE, can further determine the evolutionary state of the donor star during the X-ray phase. Moreover the value of  $\alpha_{\text{CE}}$  determines the orbital velocity and the global velocity of the post-CE binary after the SN, hence the spatial offset of the system. So different choices of  $\alpha_{\text{CE}}$  may give different  $L_X$  vs.  $R$  distributions, as already illustrated in Zuo & Li (2010). However the greatest limitation in the paper is the oversimplified treatment of CE, especially the parameter  $\lambda$ , due to the lack of an easy-to-use fitting formulae of  $\lambda$  at that time, as discussed in the paper.

In the present work, we applied a most up-to-date BPS technique to revisit the  $L_X$  vs.  $R$  problem. The updates include several folds, with two crucial for the CE phase (i.e., variable  $\lambda$  and a new CE criterion for Hertzsprung gap (HG) donor stars, see §2.1.1). The main goal of this study is to see whether the  $L_X$  vs.  $R$  correlation could be reconstructed within the range of reasonable value of  $\alpha_{\text{CE}}$ , given the current knowledge of CE evolution. We present the  $L_X$  vs.  $R$  distribution under different choices of  $\alpha_{\text{CE}}$ , by comparing with observations, to constrain the value of  $\alpha_{\text{CE}}$ . The well simulated  $L_X$  vs.  $R$  distribution can also help to understand the nature of the sources and may be testified by future high-resolution X-ray and optical observations.

This paper is organized as follows. In §2 we describe the BPS method and the input physics for X-ray binaries (XRBs) in our model. The calculated results and discussions are presented in §3. Our conclusions are in §4.

## 2 MODEL DESCRIPTION

### 2.1 Assumptions and input parameters

#### 2.1.1 binary evolution

To follow the evolution of HMXBs, we have used the BPS code initially developed by Hurley et al. (2000, 2002) and recently updated by Zuo, Li & Gu (2014a) in our calculation. In the present code, the compact object masses are calculated using a prescription same as in Fryer et al. (2012, i.e., the rapid supernova mechanism), which can model the mass distribution of neutron stars (NSs) and black holes (BHs) in the Galactic XRBs quite well (Belczynski et al. 2012). We also consider the formation of NSs through electron capture supernovae (i.e. ECS, Podsiadlowski et al. 2004). The maximum NS mass is assumed to be  $2.5 M_{\odot}$ , above which black hole (BH) is assumed to form. We account for fallback and direct BH formation during core collapse (Fryer & Kalogera 2001). The mass loss prescription for the winds in massive stars has also been updated (Vink et al. 2001, also see Belczynski et al. 2010).

Following Zuo & Li (2010), we adopt a constant star formation rate for a duration of 20 Myr, in parallel with Kaaret et al. (2004), to model the HMXB populations. We construct several models, in each model, we evolve  $8 \times 10^6$  primordial systems, all of which are initially binary systems. We set up the same grid of the initial parameters (i.e., the primary mass, secondary mass and orbital separation) as Hurley et al. (2002) and evolve each binary then. In the following we describe the assumptions and input parameters in our basic model (i.e., model A09 in Table 1, equivalent to model M1 in Table 2).

#### (1) initial parameters

We adopt the initial mass function (IMF) of Kroupa (2001, hereafter KROUPA01 for short) for the distribution of the primary mass ( $M_1$ ). For the secondary's mass ( $M_2$ ), a power law distribution of the mass ratio  $P(q) \propto q^{\alpha}$  is assumed, where  $q \equiv M_2/M_1$ . In our basic model, a flat distribution is assumed, i.e.  $\alpha = 0$ . Finally a uniform distribution is also taken for the logarithm of the orbital separation (i.e.,  $\ln a$ ).

#### (2) CE evolution

The stability of mass transfer in binaries depends on both the mass ratio and the evolutionary states of both stars. Often a critical ratio of the donor mass to the accretor mass,  $q_{\text{crit}}$ , is defined, above which mass transfer is dynamically unstable between the two components. The ratio  $q_{\text{crit}}$  usually varies with the evolutionary state of the donor star at the onset of RLOF (Hjellming & Webbink 1987; Webbink 1988; Podsiadlowski et al. 2002; Chen & Han 2008). In this study, we adopt an updated  $q_{\text{crit}}$  (which was numerically calculated for a large number of binaries by use of an updated version of the Eggleton (1971, 1972)'s stellar evolution code) for CE initiated by HG donor stars (Shao & Li 2014, also see the Appendix A in Zuo, Li & Gu 2014a). If the primordial primary is on the first giant branch (FGB) or the asymptotic giant branch (AGB), we use

$$q_{\text{crit}} = [1.67 - x + 2(\frac{M_{\text{c1}}}{M_1})^5]/2.13 \quad (1)$$

where  $M_{\text{c1}}$  is the core mass of the donor star, and  $x = d \ln R_1 / d \ln M$  is the mass-radius exponent of the donor star. If the donor star is a naked helium giant,  $q_{\text{crit}} = 0.784$  (see Hurley et al. 2002, for more details).

Usually the CE interaction is parameterized in terms of the orbital energy and the binding energy. It is expressed as  $E_{\text{bind}} \equiv \alpha_{\text{CE}} \Delta E_{\text{orb}}$  (Webbink 1984, 2008), where the CE parameter  $\alpha_{\text{CE}}$  describes the efficiency of converting orbital energy ( $E_{\text{orb}}$ ) into kinetic energy, to expel the CE, and  $E_{\text{bind}}$  is the binding energy of the envelope. We adopt the standard energy prescription presented by Kiel & Hurley (2006) to compute the outcome of the CE phase<sup>1</sup>,

$$\alpha_{\text{CE}} \left( \frac{GM_c M_2}{2a_f} - \frac{GM_c M_2}{2a_i} \right) = - \frac{GM_1 M_{\text{env}}}{R_{L1} \lambda}, \quad (2)$$

which yields the ratio of final (post-CE) to initial (pre-CE) orbital separations as

$$\frac{a_f}{a_i} = \frac{M_c M_2}{M_1} \frac{1}{M_c M_2 / M_1 + 2M_{\text{env}} / (\alpha_{\text{CE}} \lambda R_{L1})}. \quad (3)$$

where  $G$  is the gravitational constant,  $M_c$  is the helium-core mass of the primary star,  $R_{L1}$  is the RL radius of the primary star,  $M_{\text{env}}$  is the mass of the primary's envelope,  $a_f$  and  $a_i$  denote the final and initial orbital separations, respectively.

Here  $\lambda$  depends on the structure of the primary star, conventionally chosen as constant (typically  $\sim 0.5$ , Hurley et al. 2002; Zuo & Li 2010) but in reality possibly far from it (Dewi & Tauris 2000; van der Sluys et al. 2006). We use the fitting formulae of envelope binding energy  $E_{\text{bind}}$  presented by Loveridge et al. (2011) which implicitly include variable  $\lambda$ . The  $E_{\text{bind}}$  is calculated by integrating the gravitational and internal energies from the core-envelope boundary to the surface of the star  $M_s$  as follows,

$$E_{\text{bind}} = \int_{M_c}^{M_s} \left( -\frac{Gm}{r(m)} \right) dm + \alpha_{\text{in}} \int_{M_c}^{M_s} E_{\text{in}} dm, \quad (4)$$

where  $E_{\text{in}}$  is the internal energy per unit of mass, containing the thermal energy of the gas and the radiation energy, but not the recombination energy (for details, see van der Sluys et al. 2006). Here we define  $\alpha_{\text{in}}$  the percentage of the internal energy contributing to the ejection of the envelope. We take its value as 1 in our basic model and change it to zero (models M6 and M13, see Table 2) for comparisons.

Note that the value of  $\lambda$  is still uncertain due to an ambiguous definition of the stellar core boundary in the literature. Here the core is defined as the central mass below the location where  $X = 10\%$  (Dewi & Tauris 2000). However other definitions are still possible to decide the boundary between the core and the envelope, for example, based on the effective polytropic index profiles (Hjellming & Webbink 1987), the change in the mass-density gradient (Bisscheroux 1988), the method suggested by Han et al. (1994), and the entropy profile (Tauris & Dewi 2001), etc. Different definitions of the core may give different values of  $\lambda$ , then translate directly similar uncertainties in the value of  $\alpha_{\text{CE}}$ . In extreme cases, the ‘entropy profile’ definition for the core can increase the value of  $\lambda$  by a factor of 10-70 for massive stars (Tauris & Dewi 2001, see also Ivanova 2011), which may be the progenitor of HMXBs, then the expected value of  $\alpha_{\text{CE}}$  will be extremely small.

<sup>1</sup> Another formulation (Webbink 1984) takes the initial orbital energy (i.e., the second term in parenthesis in Eq. 2) to be  $-\frac{GM_1 M_2}{2a_i}$ , but gives negligible difference in the final results.

We consider several different choices of  $\alpha_{\text{CE}}$  (see Table 1) in order to constrain the value in our calculations. The two extreme values of  $\alpha_{\text{CE}}$  are adopted as 0.2 and 1.0, since firstly  $\alpha_{\text{CE}}$  should be within unity as we have considered the potential internal energies in the quantity of  $E_{\text{bind}}$ , and secondly the value of  $\alpha_{\text{CE}} < \sim 0.1$  is likely excluded according to our HMXB XLF modeling (Zuo & Li 2014b). These models are denoted as A02-A10, respectively, where the last two digits correspond to the value of  $\alpha_{\text{CE}}$ , and we set A09 as our basic model according to our calculations.

### (3) SN kicks

The newborn NS/BH in HMXBs may receive different velocity kicks. For NS systems, the kick velocity  $v_k$  is assumed to follow a Maxwellian distribution

$$P(v_k) = \sqrt{\frac{2}{\pi}} \frac{v_k^2}{\sigma_{\text{kick}}^3} \exp\left(-\frac{v_k^2}{2\sigma_{\text{kick}}^2}\right), \quad (5)$$

and we adopt  $\sigma_{\text{kick}} = 150 \text{ km s}^{-1}$  in our basic model though its value is still very uncertain. For BH systems, the natal kicks are assumed to be multiplied by a factor of  $(1-f_b)$  if formed with partial mass fallback, where  $f_b$  is the fraction of the stellar envelope that falls back after the SN explosion. Specially BHs formed with small amounts of fall back ( $M_{\text{fb}} < 0.2 M_{\odot}$ ) are assumed to receive full kicks. In situations where BHs form silently (without a SN explosion) via direct collapse, no natal kick is adopted (Fryer et al 2012; Dominik et al. 2012). Additionally, for ECS NSs, no kick velocity is assumed since these are weak SN occurring for the lowest stars ( $M_{\text{ZAMS}} = 7.6 - 8.3 M_{\odot}$ , Hurley et al. 2000; Eldridge & Tout 2004a,b; Belczynski et al. 2008).

The velocity ( $\mathbf{v}_{\text{sys}}$ ) of the binary system after the SN is determined by both the natal kick and the orbital velocity of the system. It can be expressed as follows (see Hurley et al. 2002, for details),

$$\mathbf{v}_{\text{sys}} = \frac{M'_1}{M'_b} \mathbf{v}_k - \frac{\Delta M_1 M_2}{M'_b M_b} \mathbf{v}, \quad (6)$$

where  $M'_1 = M_1 - \Delta M_1$  is the current mass of the primary star after losing mass  $\Delta M_1$  during the SN,  $M_b = M_1 + M_2$  and  $M'_b = M_b - \Delta M_1$  are the total masses of the system before and after the SN, respectively;  $\mathbf{v}$  is the relative orbital velocity of the stars (see Eq. A1 in Hurley et al. 2002). Tidal effect is also taken into account to remove any eccentricity induced in a post-SN binary prior to the onset of mass transfer.

Several key parameters may affect the  $L_X$  vs.  $R$  distribution, such as the IMFs of the primary and secondary stars, the natal kick velocity, etc. (see Zuo & Li 2010, for more details and references therein). So we also adopt a top flatter IMF of Matteucci & Tornambè (1987, hereafter MT87, models M2 and M9), a ‘twins’ model (i.e.,  $\alpha = 1$ , models M3 and M10) and a higher dispersion of kick velocity  $\sigma_{\text{kick}} = 265 \text{ km s}^{-1}$  (i.e., models M4 and M11, Hobbs et al. 2005) to test their effects. Two additional models with  $\alpha = -1$  ( $0.1 \leq q \leq 1.0$ ) and orbital distribution  $(\ln a)^{-0.45}$  (Sana et al. 2013) have also been examined, the results of which are similar to that of our basic model. Additionally, stronger wind mass loss may reduce the envelope mass sufficiently, avoiding the occurrence of CE or CE mergers (Soker 2004), so we adopt a wind mass loss rate enhanced by a factor of two to test the effect (models M7 and M14). During the mass transfer phase, mass and angular momentum

**Table 1.** Different models on the treatment of the CE parameters  $\alpha_{\text{CE}}$ .

Model	A02	A03	A04	A05	A06	A07	A08	A09	A10
$\alpha_{\text{CE}}$	0.2	0.3	0.4	0.5	0.6	0.7	0.8	0.9	1.0

**Table 2.** Parameters adopted for each model. Here  $\alpha_{\text{CE}}$  is the CE parameter,  $q$  is the initial mass ratio,  $\sigma_{\text{kick}}$  is the dispersion of kick velocity, IMF is the initial mass function,  $\alpha_{\text{in}}$  represents the percentage of the internal energy contributing to the ejection of the envelope, STDw is the standard stellar winds, while STGw represents the standard wind mass-loss rate increased to 200 per cent, STDm is the standard mass transfer rate (MTR) before the CE, while REDm represents the standard MTR reduced to 50 per cent.

Model	$\alpha_{\text{CE}}$	P(q)	$\sigma_{\text{kick}}$ km/s	IMF	$\alpha_{\text{in}}$	winds	MTR
M1	0.9	$\propto q^0$	150	KROUPA01	1	STDw	STDm
M2	0.9	$\propto q^0$	150	MT87	1	STDw	STDm
M3	0.9	$\propto q^1$	150	KROUPA01	1	STDw	STDm
M4	0.9	$\propto q^0$	265	KROUPA01	1	STDw	STDm
M5	0.9	$\propto q^0$	150	KROUPA01	1	STDw	REDm
M6	0.9	$\propto q^0$	150	KROUPA01	0	STDw	STDm
M7	0.9	$\propto q^0$	150	KROUPA01	1	STGw	STDm
M8	0.2	$\propto q^0$	150	KROUPA01	1	STDw	STDm
M9	0.2	$\propto q^0$	150	MT87	1	STDw	STDm
M10	0.2	$\propto q^1$	150	KROUPA01	1	STDw	STDm
M11	0.2	$\propto q^0$	265	KROUPA01	1	STDw	STDm
M12	0.2	$\propto q^0$	150	KROUPA01	1	STDw	REDm
M13	0.2	$\propto q^0$	150	KROUPA01	0	STDw	STDm
M14	0.2	$\propto q^0$	150	KROUPA01	1	STGw	STDm

loss rates may also affect the following CE, so we assume half of the transferred mass lost in models M5 and M12 (see Table 2).

### 2.1.2 binary motion

Since a star cluster in a star-burst region is usually centrally concentrated, we assume a spherical potential and use the cylindrical coordinate system  $(r, \phi, z)$  centered at the cluster's center. The potential of a cluster can be described as

$$\Phi(r, z) = \frac{-GM}{\sqrt{r^2 + z^2 + h}}, \quad (7)$$

where  $h$  is the half light radius and  $M$  is the total mass of stars within  $h$ . For typical star clusters we adopt  $M = 1.0 \times 10^6 M_{\odot}$ , and  $h = 3$  pc (Ho & Filippenko 1996a,b) in our calculations<sup>2</sup>. Then all stars are assumed to born uniformly in the star cluster. The direction of its initial velocity is randomly designated, which gives the initial velocity vectors  $v_r, v_{\phi}, v_z$ . Because of the cylindrical symmetry of cluster potential, two space coordinates  $r$  and  $z$  are sufficient to describe the HMXB distributions. We then integrate the motion equations (see Equations 19a and 19b in Paczyński 1990) with a fourth-order Runge-Kutta method to calculate the trajectories of the binary systems and collect the parameters of current XRBs if turning on X-rays. Finally the positions of XRBs are projected on the  $\phi = 0$

plane to get the projected distances from star clusters, i.e.,  $R = ((r \cos \varphi)^2 + z^2)^{1/2}$  with  $\varphi$  uniformly distributed between 0 and  $2\pi$ . In our calculations, the accuracy of integral is set to be  $10^{-6}$  and controlled by the energy integral.

### 2.2 X-ray luminosity and source type

We use the same methods to compute the 0.5 – 8 keV X-ray luminosity of different HMXB populations as in Zuo, Li & Gu (2014a). In this study, we do not consider low-mass X-ray binaries (LMXBs, donor mass  $< 2 M_{\odot}$ ) since it takes  $\sim$  Gyr for them to form, much longer than the duration time we considered. Every accreting HMXB is usually powered by either accretion disk or stellar winds. We use the classical Bondi & Hoyle (1944)'s formula to calculate the mass transfer rate for wind-fed systems. In the case of disk accretion, the material is transferred to the compact star by Roche-lobe overflow (RLOF). We discriminate persistent and transient sources using the criteria of Lasota (2001, i.e., Eq 36 therein) for MS and red giant stars in RLOF cases. The simulated X-ray luminosity is described as follows:

$$L_{\text{X},0.5-8\text{keV}} = \begin{cases} \eta_{\text{bol}} \eta_{\text{out}} L_{\text{Edd}} & \text{transients in outbursts} \\ \eta_{\text{bol}} \min(L_{\text{bol}}, \eta_{\text{Edd}} L_{\text{Edd}}) & \text{persistent systems,} \end{cases} \quad (8)$$

where  $L_{\text{bol}} \simeq 0.1 \dot{M}_{\text{acc}} c^2$  where  $\dot{M}_{\text{acc}}$  is the average mass accretion rate and  $c$  the speed of light;  $\eta_{\text{bol}}$  is the bolometric correction factor which converts the bolometric luminosity ( $L_{\text{bol}}$ ) to the 0.5 – 8 keV X-ray luminosity, adopted as 0.2 for NS-XRBs and 0.4 for BH-XRBs, respectively

<sup>2</sup> We also reduced the cluster mass to 50%, and found no significant difference in the final results.

though its range is  $\sim 0.1 - 0.8$  for different types of XRBs (Belczynski et al. 2008); the critical Eddington luminosity  $L_{\text{Edd}} \simeq 4\pi GM_1 m_p c / \sigma_T = 1.3 \times 10^{38} m_1 \text{ erg s}^{-1}$  (where  $\sigma_T$  the Thomson cross section,  $m_p$  the proton mass, and  $m_1$  the accretor mass in the units of solar mass).  $\eta_{\text{Edd}}$  is called as the ‘Begelman’ factor which examines the allowed maximum super-Eddington accretion rate. Here we adopt  $\eta_{\text{Edd,NS}} = 5$  for NS XRBs and  $\eta_{\text{Edd,BH}} = 100$  for BH XRBs in our calculation (Zuo, Li & Gu 2014a). For transient sources the outburst luminosity is taken as a fraction ( $\eta_{\text{out}}$ ) of the critical Eddington luminosity. We take  $\eta_{\text{out}} = 0.1$  and 1 for NS and BH transients with orbital period  $P_{\text{orb}}$  less and longer than 1 day and 10 hr, respectively (Chen et al. 1997; Garcia et al. 2003; Belczynski et al. 2008).

The Be/X-ray binary (Be-XRB) is also included in our calculation. It contains a Be companion, usually accreted by an orbiting NS at its periastron, showing as X-ray transients. Five criterions are set to define it in a phenomenological way as in Zuo, Li & Gu (2014a, also see Belczynski & Ziolkowski, 2009). Technically, we randomly selected only 25% ( $f_{\text{Be}} = 0.25$ , Slettebak 1988; Ziolkowski 2002; McSwain & Gies 2005) of NS binaries hosting a massive ( $3.0 M_{\odot} - 20.0 M_{\odot}$ ) B/O star to predict their numbers. The X-ray luminosity of a Be-XRB is calculated using Eq. 11 in Dai et al. (2006), which is based on data compiled by Raguzova & Popov (2005). Due to the transient characteristics ( $\sim 0.2 - 0.3 P_{\text{orb}}$ , Reig 2011), we adopt  $DC_{\text{max}} = 0.3$  to give the maximum expected numbers.

### 3 RESULTS

Based on a population of 66 X-ray point sources, Kaaret et al. (2004) studied the spatial offsets between these sources and the star clusters in three starburst galaxies (i.e., M82, NGC 1569 and NGC 5253). They found that the X-ray sources are preferentially located near the star clusters, with the brighter sources closer to the clusters. Moreover, they found no luminous source ( $L_X > 10^{38} \text{ erg s}^{-1}$ ) at relatively large displacements ( $> 200 \text{ pc}$ ) from the clusters. Here we modeled the kinematic evolution of XRBs in clusters, and presented the results below.

As stated before several models are constructed to investigate how the final results are impacted by the CE parameter  $\alpha_{\text{CE}}$ . In practice, the following steps are performed to make the comparison. Step (I), the average source displacement distributions are calculated using the observed data. We restrict the source luminosities to the range of  $10^{36} - 10^{38} \text{ erg s}^{-1}$  in order to compare with Kaaret et al. (2004). Step (II), a two-dimensional Kolmogorov-Smirnov (2D K-S) test is performed, to compare the simulated displacement distributions with the average displacement derived in step I. This way, we can get a preliminary decision for the parameter  $\alpha_{\text{CE}}$ , by seeing the derived possibility (i.e.,  $p$ -value, see Tables 3 and 4. The value of  $p$  that is less than  $\sim 0.01$  suggests a significant different distribution.). Step (III), the  $L_X$  vs.  $R$  distribution gives the occurrence possibilities of sources in each region, direct 2D K-S test with discrete sources is likely impossible, so we use it in a phenomenological way to further discriminate between models (i.e., the secondary check for the models).

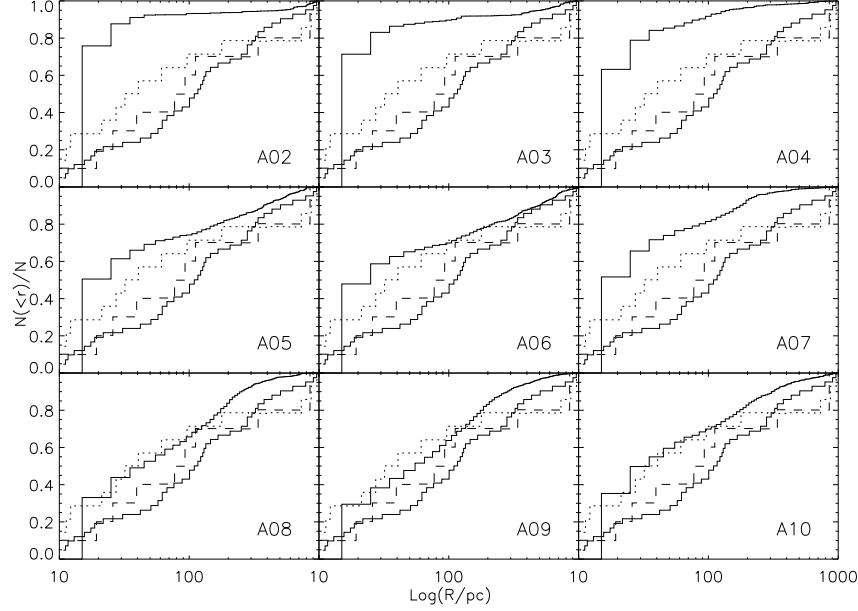
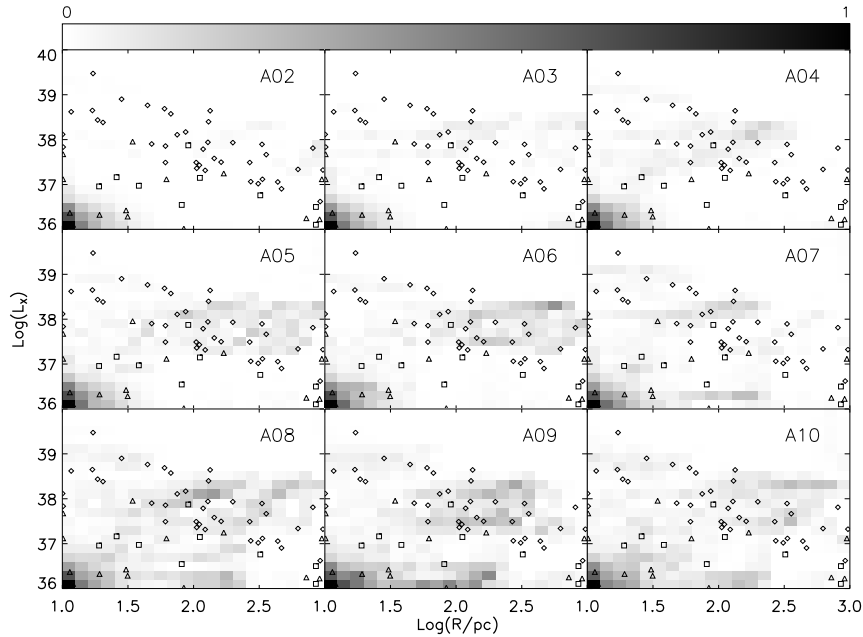
Fig. 1 shows the simulated cumulative distribution of

the XRB displacements at the age of 20 Myr for models A02-A10, respectively. We normalized each histogram by the total number of HMXBs in the 10-1000 pc region. Our results show that models with  $\alpha_{\text{CE}}$  between  $\sim 0.8 - 1.0$  can match the observation (e.g., Fig. 2 in Kaaret et al. 2004) quite closely, while models with  $\alpha_{\text{CE}} < \sim 0.4$  (possibilities  $< 10^{-6}$ , see Table 3) clearly fail. It shows that very few sources can move to 100 pc away from the star clusters, which is in marked contrast with the observations. Models A05-A07, with possibilities  $\sim 10^{-1}$ , can not be firmly ruled out. Further model-check comes from Fig. 2 for the simulated distributions of X-ray luminosities ( $L_X$ ) at different displacements ( $R$ ) from the star cluster in models A02-A10, respectively. The color bar represents the normalized number ratio of HMXBs in the  $L_X - R$  plane. Note that the predicted  $L_X$  vs.  $R$  correlation in models A08-A10 are compatible with the observations quite well, while others likely fail, especially for models A02-A04, the  $L_X$  vs.  $R$  correlation can hardly be reconstructed. We find that this result is also consistent with the one obtained through HMXB XLF simulations recently presented by Zuo & Li (2014b). Recently Ivanova & Chaichenets (2011) suggested a modified approach to the standard energy CE model, i.e., ‘enthalpy’ prescription. A non-negative energy (i.e.,  $P/\rho$ ) is considered additionally to unbind the envelope. This may mean a decrease of the binding energy of the envelope, and hence the required CE efficiency  $\alpha_{\text{CE}}$ , or an increase of the portion of the orbital energy used to eject the CE, equivalent to increase the effective value of  $\alpha_{\text{CE}}$ . Therefore the range of  $\alpha_{\text{CE}}$  we obtained here still suffers from uncertainties. According to Ivanova & Chaichenets (2011), the variation ratios in most giants are from  $\sim 2$  to  $\sim 5$ .

In order to further check the constraints on the value of  $\alpha_{\text{CE}}$ , we also adopt several models with different assumptions under two typical values of  $\alpha_{\text{CE}}$  ( $\alpha_{\text{CE}} = 0.9$  for models M1-M7 and  $\alpha_{\text{CE}} = 0.2$  for models M8-M14, see Table 2). The results are presented in Fig. 3 (cumulative distributions, same as in Fig. 1) and Fig. 4 ( $L_X$  vs.  $R$  distributions, same as in Fig. 2), respectively. One can see that models with  $\alpha_{\text{CE}} = 0.9$  (i.e., models M1-M6 except M7, possibility  $\sim 10^{-4}$ , see Table 4) can match the observation generally while models with  $\alpha_{\text{CE}} = 0.2$  (i.e., models M8-M14) still fail. We note that models M8-M14 all have extremely small possibilities except models M12 and M13, both of which are further ruled out by the  $L_X$  vs.  $R$  distributions. Stronger stellar wind (i.e., models M7 and M14) leads to too few HMXBs, as well as ones at large displacements, which is not comparable with observations, so we do not give further discussions on it but only present the corresponding informations for reference. Note that models M1-M6 all have similar  $L_X$  vs.  $R$  correlations which are constructed by both BH-XRBs and NS-XRBs. It is clear from Fig. 4 that BH-XRBs mainly dominate at small-offset ( $10 < R < 100 \text{ pc}$ ) regions, with luminosities covering a broad range, from high luminosities ( $L_X > 10^{38} \text{ erg s}^{-1}$ , named as regions A), to low luminosities ( $10^{36} < L_X < 10^{38} \text{ erg s}^{-1}$ , named as regions B). While NS-XRBs spread in much broader spatial regions, as far as about 1 kpc, however their maximum luminosities are relatively lower than that of BH-XRBs in all of the models, due to a lower Eddington accretion rate limit, as expected. Similarly we define the regions with the spatial offset of  $100 < R < 1000 \text{ pc}$  as region C in order for fur-

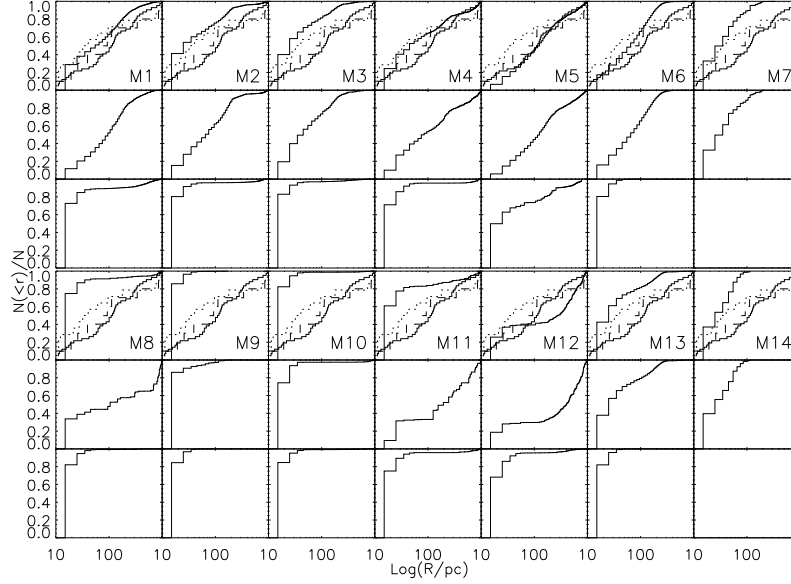
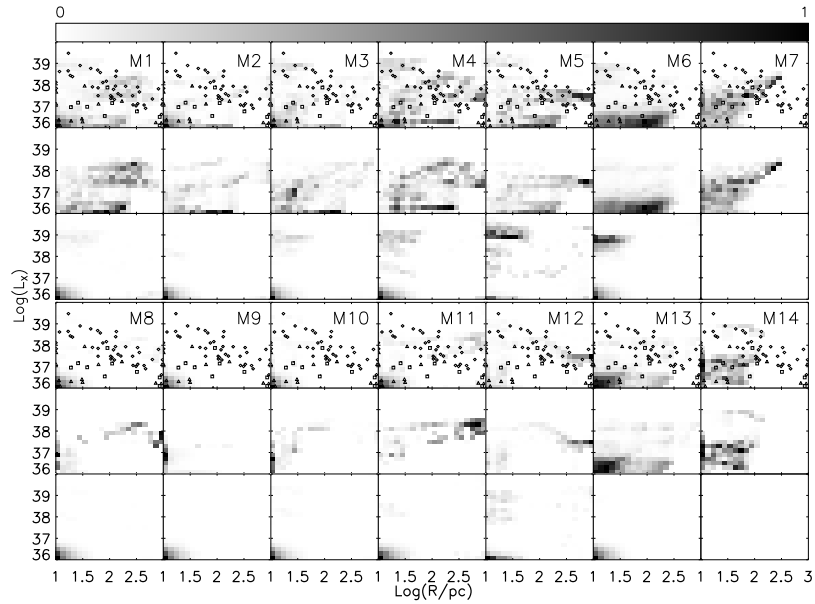
**Table 3.** Two-dimensional K-S test for models A02-A10.

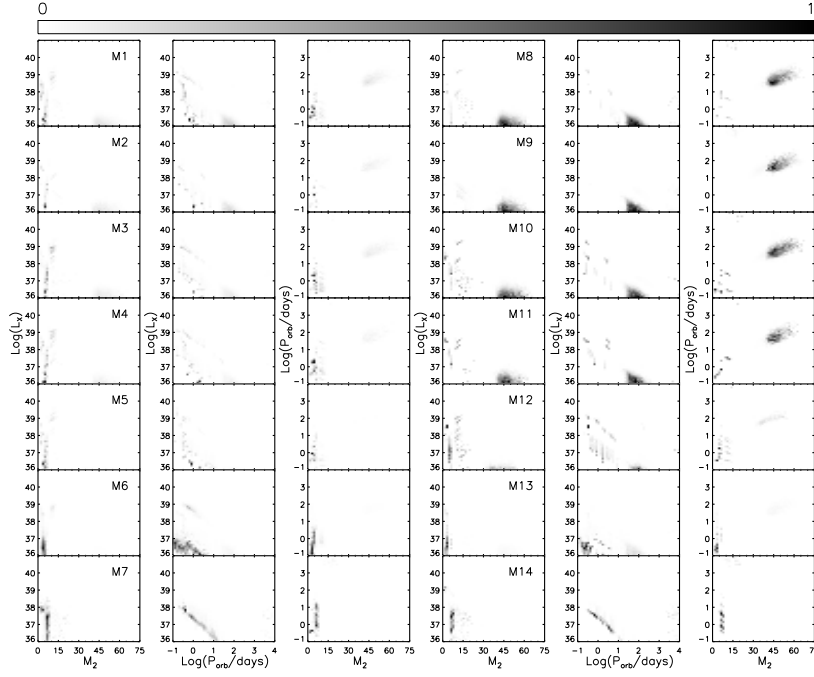
Model	A02	A03	A04	A05	A06	A07	A08	A09	A10
$p$ -value	$3 \times 10^{-7}$	$8 \times 10^{-7}$	$8 \times 10^{-6}$	0.05	0.18	0.02	0.31	0.45	0.43

**Figure 1.** The normalized cumulative distribution (thick-solid line) for models A02-A10, respectively (see Table 1). The thin-solid, dotted and dashed lines represent the observed cumulative distributions of source displacements in galaxies M82, NGC 1569 and NGC 5253 (see Fig. 2 in Kaaret et al. 2004), respectively.**Figure 2.** The  $L_X - R$  distribution for models A02-A10 (see Table 1), respectively. Sources from M82, NGC 1569 and NGC 5253 in Kaaret et al. (2004, see Fig. 3) samples are also shown as diamonds, triangles and squares, respectively for comparison.

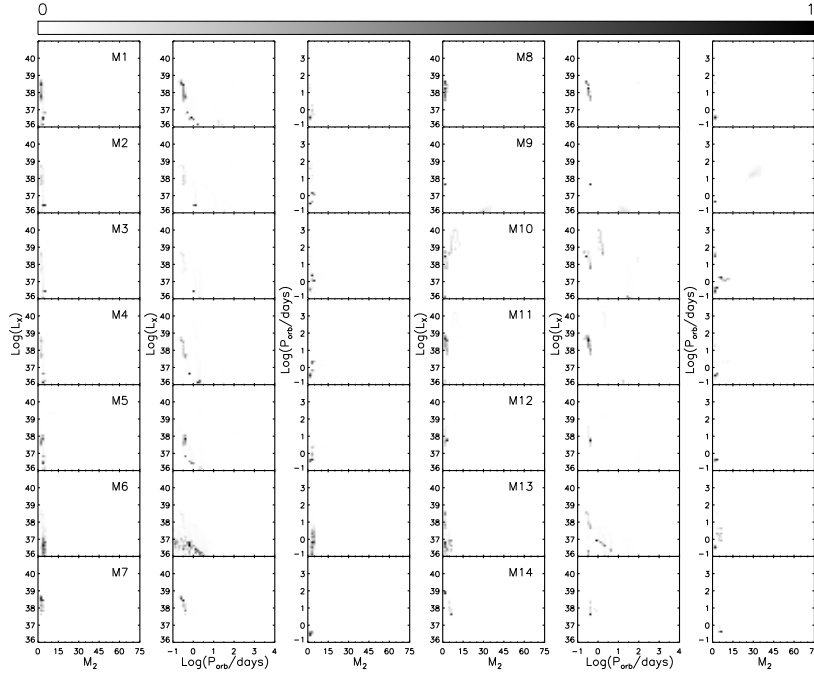
**Table 4.** Two-dimensional K-S test for models M1-M14.

Model	M1	M2	M3	M4	M5	M6	M7
<i>p</i> -value	0.45	0.07	0.04	0.9	0.8	0.2	$2 \times 10^{-4}$
Model	M8	M9	M10	M11	M12	M13	M14
<i>p</i> -value	$3 \times 10^{-7}$	$2 \times 10^{-8}$	$2 \times 10^{-8}$	$6 \times 10^{-5}$	$1 \times 10^{-2}$	$8 \times 10^{-3}$	$8 \times 10^{-6}$


**Figure 3.** The normalized cumulative distribution for the numbers of ALL-XRBs (top), NS-XRBs (middle) and BH-XRBs (bottom) in models M1-M7 (upper panel) and M8-M14 (lower panel), respectively. The thin-solid, dotted and dashed lines represent the observed cumulative distributions of source displacements in galaxies M82, NGC 1569 and NGC 5253 (see Fig. 2 in Kaaret et al. 2004), respectively.

**Figure 4.** The  $L_X - R$  distribution for ALL-XRBs (top), NS-XRBs (middle) and BH-XRBs (bottom) in models M1-M7 (upper panel) and M8-M14 (lower panel), respectively. Sources from M82, NGC 1569 and NGC 5253 in Kaaret et al. (2004, see their Fig. 3) samples are also shown as diamonds, triangles and squares, respectively for comparison.



**Figure 5.** The  $L_X - M_2$ ,  $L_X - P_{\text{orb}}$ , and  $P_{\text{orb}} - M_2$  distributions in the  $10 < R < 100$  pc region for models M1-M7 (left three columns, from top to bottom) and models M8-M14 (right three columns, from top to bottom), respectively.



**Figure 6.** Same as in Fig. 5 but for sources in the region of  $100 < R < 1000$  pc (regions C).

ther analysis. We emphasize here that different regions in the  $L_X - R$  plane are occupied by different populations of HMXBs, for example regions A generally BH-XRBs, regions C NS-XRBs, however regions B are dominated by both NS and BH XRBS.

In order to explore the nature of XRBS in different regions, we also examined their observational properties, such as current mass  $M_2$  and spectral type of the donor star, orbital period  $P_{\text{orb}}$ , and system velocity distributions. Fig-

ures 5 and 6 show the  $L_X - M_2$ ,  $L_X - P_{\text{orb}}$ , and  $P_{\text{orb}} - M_2$  distributions of XRBS for models M1-M7 (left three columns, from top to bottom) and M8-M14 (right three columns, from top to bottom) in the region of  $10 < R < 100$  pc (i.e., regions A and B) and  $100 < R < 1000$  pc (regions C), respectively. The detailed source types in regions A, B and C for models M1-M14 are listed in Tables 5-7, respectively.

Fig. 5 shows that the XRBS in region A are in short orbital periods (several hours to  $\sim 1$  day), with donors



**Table 5.** The detailed types of sources in region A ( $L_X > 10^{38} \text{ erg s}^{-1}$ ,  $10 < R < 100 \text{ pc}$ ). Here BH per cent represents the percentage of BH-XRBs in region A,  $\frac{N(>10^{38} \text{ erg/s})}{N(>10^{36} \text{ erg/s})}$  represents the percentage of high-luminosity ( $L_X > 10^{38} \text{ erg s}^{-1}$ ) sources in  $10 < R < 100 \text{ pc}$  region. “BH(NS)MS” and “BH(NS)HeMS” represent BH(NS)-XRBs with MS companions and BH(NS)-XRBs with HeMS companions, respectively.

Model	BH per cent	$\frac{N(>10^{38} \text{ erg/s})}{N(>10^{36} \text{ erg/s})}$	BHMS BH	BHHeMS BH	NSMS NS	NSHeMS NS
M1	67	14	0	99	100	0
M2	37	7	1	99	95	5
M3	90	17	0	99	81	19
M4	67	21	1	99	92	8
M5	61	16	0	99	95	5
M6	39	10	1	99	10	90
M7	0	7	0	0	49	51
M8	72	2	0	99	100	0
M9	86	0	100	0	100	0
M10	51	8	0	99	95	5
M11	53	11	0	99	97	3
M12	54	23	1	99	98	2
M13	1	10	1	99	16	84
M14	0	6	0	0	16	84

**Table 6.** Same as in Table 5 but for sources in region B ( $10^{36} < L_X < 10^{38} \text{ erg s}^{-1}$ ,  $10 < R < 100 \text{ pc}$ ). Here  $\frac{N(10^{36} < L_X < 10^{38} \text{ erg/s})}{N(>10^{36} \text{ erg/s})}$  represents the percentage of low-luminosity ( $10^{36} < L_X < 10^{38} \text{ erg s}^{-1}$ ) sources in  $10 < R < 100 \text{ pc}$  region.

Model	BH per cent	$\frac{N(10^{36} < L_X < 10^{38} \text{ erg/s})}{N(>10^{36} \text{ erg/s})}$	BHMS BH	BHHeMS BH	NSMS NS	NSHeMS NS
M1	42	86	99	0	26	74
M2	50	93	99	1	12	88
M3	32	83	98	2	9	91
M4	22	79	88	12	3	97
M5	3	84	56	44	7	93
M6	3	90	94	6	1	99
M7	0	93	0	0	49	51
M8	91	98	99	1	69	31
M9	91	100	100	0	100	0
M10	61	92	64	36	71	29
M11	89	89	99	0	34	66
M12	37	77	87	13	30	70
M13	16	90	100	0	2	98
M14	0	94	0	0	23	77

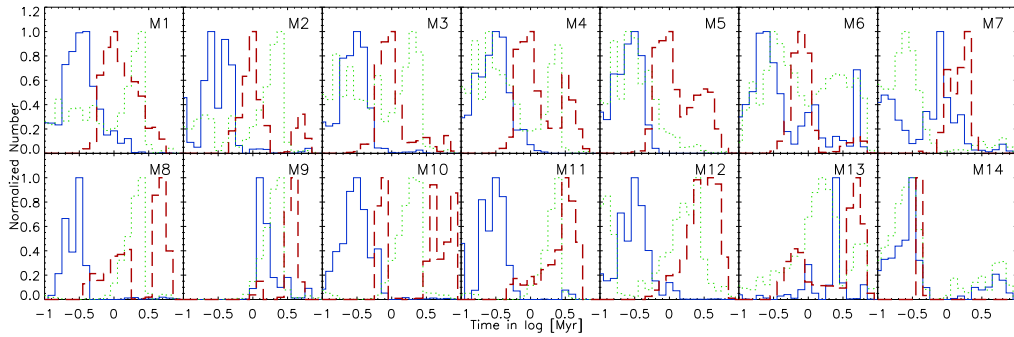


**Figure 7.** The delay time distributions between SN and the turning-on of X-rays for sources in regions A (solid line), B (dotted line) and C (thick dashed line), respectively. From left to right are models M1-M7 (upper panel) and M8-M14 (lower panel), respectively.

**Table 7.** Same as in Table 5 but for sources in region C ( $L_X > 10^{36} \text{ erg s}^{-1}$ ,  $100 < R < 1000 \text{ pc}$ ).  $\frac{N(>10^{38} \text{ erg/s})}{N(>10^{36} \text{ erg/s})}$  represents the percentage of high-luminosity ( $L_X > 10^{38} \text{ erg s}^{-1}$ ) sources in region C.

Model	BH	per cent	$\frac{N(>10^{38}\text{erg/s})}{N(>10^{36}\text{erg/s})}$	$\frac{\text{BHMS}}{\text{BH}}$	$\frac{\text{BHHeMS}}{\text{BH}}$	$\frac{\text{NSMS}}{\text{NS}}$	$\frac{\text{NSHeMS}}{\text{NS}}$
M1	6	26	2	98	70	30	
M2	7	22	5	95	45	55	
M3	6	20	42	57	28	72	
M4	3	25	51	49	48	52	
M5	2	8	30	70	53	47	
M6	1	4	4	96	2	98	
M7	0	74	0	0	21	79	
M8	6	65	5	95	100	0	
M9	0	0	0	0	100	0	
M10	61	69	64	36	100	0	
M11	13	79	37	63	100	0	
M12	3	14	47	53	91	1	
M13	0	5	0	0	13	87	
M14	0	64	0	0	0	100	

around several solar masses to  $\sim 15 M_\odot$  for all models. They are mainly BH-XRBs with helium main-sequence (HeMS) donors and NS-XRBs with main-sequence (MS) companions (see Table 5). The binary velocities are  $\sim 100 - 200 \text{ km s}^{-1}$  for all models. Considering that they have relative short evolutionary time-scales (generally  $\sim 0.5 \text{ Myr}$ , see Fig. 7), they can not move too far, even not farther than  $100 \text{ pc}$ . The XRBs in region B however show some diversities. They can be further divided into two subgroups, one with relative short orbital periods (about days) and less massive ( $< 10 M_\odot$ ) companions, while the other with donors much more massive ( $\sim 30 - 60 M_\odot$ ) and orbits much wider (periods about tens of days to even hundreds of days). Further analysis indicates that the former group is mainly NS-XRBs, with relative high speed which peaks at  $\sim 200 \text{ km s}^{-1}$ , while the latter one is mainly low-speed ( $< 30 \text{ km s}^{-1}$ ) BH-XRBs, which are powered by stellar winds from massive MS donors, dominating at the low luminosity range ( $\sim 10^{36} - 10^{37} \text{ erg s}^{-1}$ ). Considering that they have similar evolutionary timescales (i.e., of the order of  $1 \text{ Myr}$ , see Fig. 7), the difference in the velocities explains the different maximum offsets of NS- and BH-XRBs in the region. Note that sources in models M8-M11 are dominated by this kind of low-speed BH-XRBs (see Table 6), which may explain why the majority of sources in these models are nearby the cluster center, and they can not match the observations. Fig. 6 shows that, the XRBs in region C all have relatively low-mass ( $< 5 M_\odot$ ) companions. Their orbital periods are around several hours to days for all models. The typical velocities are  $\sim 150 - 300 \text{ km s}^{-1}$ , larger than those of high-luminosity sources. Considering that they also have relatively longer evolutionary timescales ( $\sim 0.5 \text{ Myr}$  in regions A versus  $\sim 1 - 10 \text{ Myr}$  in regions C, see Fig. 7), both the two aspects determine that they can move much farther than sources in regions A. We may see from above that, besides the system velocities at the moment of SN explosion, the spatial offsets of XRBs also depends on the delay time from the SN to the onset of X-rays. So in Fig. 7 we present the distribution of the delay time for sources in regions A (solid line), B (dotted line) and C (thick dashed line), respectively.

We normalize each the histograms by the total number of X-ray sources in each region. It is clear that sources in regions A have the shortest evolutionary timescales, while the timescales in regions B and C distribute more broadly. We note sources in regions C may reach the longest evolutionary timescales, especially for sources in models M8-M13, however they are rare.

We note that the differences of binary velocities among models are still tightly related to the companion masses  $M_{2,\text{SNe}}$ , and the orbital periods  $P_{\text{orb,SNe}}$  (or orbital velocity) at the moment of SN explosions (see Eq. 5), as already stated in Zuo & Li (2010). The CE parameter  $\alpha_{\text{CE}}$ , as a key parameter that affects the binary orbit, can not only determine the types of XRB populations, but also affect the orbital velocity immediately after the CE, hence the global velocity of the binary system. These phenomena are demonstrated clearly in Fig. 8, i.e., the  $P_{\text{orb,SNe}} - M_{2,\text{SNe}}$  distribution in regions A, B and C for models M1-M7 (upper panel) and M8-M14 (lower panel), respectively.

It is clear that short period pre-SN systems in models M8-M13 are much less than in models M1-M6, resulting in much less high speed sources. It is because of the fact that larger values of  $\alpha_{\text{CE}}$  (i.e., models M1-M6) can prevent coalescence of a NS/BH and the companion in a compact binary during the unstable mass transfer processes, in favor of the formation of tight XRBs, hence more sources with larger orbital and system velocities. While it is not the case for models M8-M13 where BH-MS XRBs dominate generally. They mainly have longer-period (hence smaller orbital velocity) and more massive companions, resulting in smaller system velocity (hence smaller offset from the parent cluster) than others. These facts clearly imply that the CE parameter  $\alpha_{\text{CE}}$ , by affecting the binary orbit, plays an important role in the kinematic motion and spatial distributions of XRBs, demonstrating itself as distinct  $L_X$  vs.  $R$  distributions. And conversely, the well measured  $L_X$  vs.  $R$  distribution can make a good decision for the precise choice of the CE parameter. Our work motivates further efforts to explore the spatial distributions of XRBs, as well as their source types in nearby star-forming galaxies.

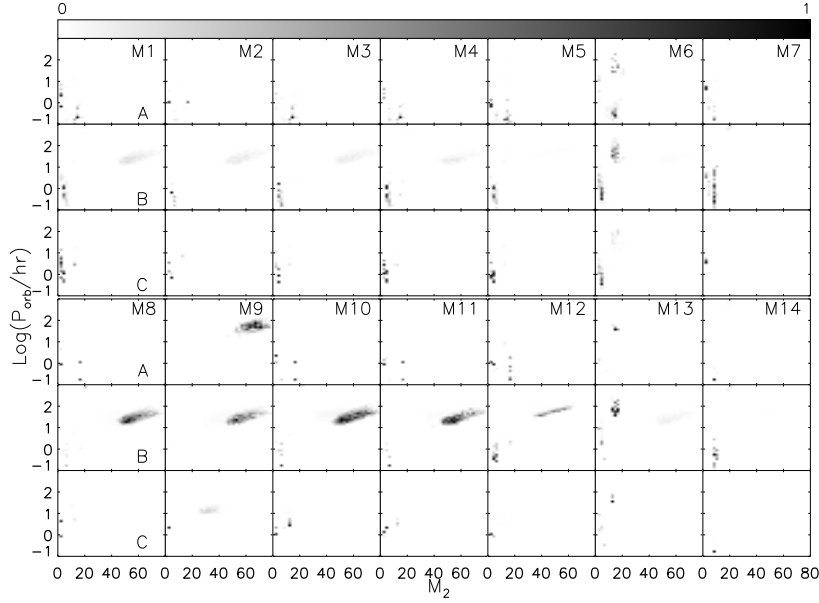


**Figure 8.** The  $P_{\text{orb,SNe}} - M_{2,\text{SNe}}$  distributions in regions A, B and C, respectively. From left to right are models M1-M7 (upper panel) and M8-M14 (lower panel), respectively.

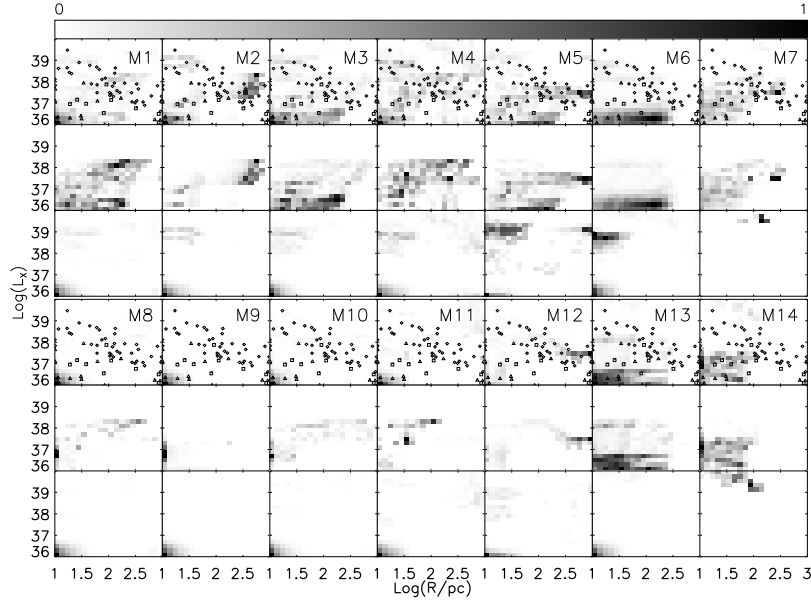


**Figure 9.** Same as in Fig. 4 but with AIC of accreting NSs considered.

We note that in the above cases, we did not consider BHs formed from accretion-induced collapse (AIC) of NS systems, however whether AIC of NSs happens or not is still in controversy. In order to examine this effect, we also consider the NS→BH AIC formation channel. The results are presented in Fig. 9, which is the same as in Fig. 4, except AIC of NSs considered here. One can see that, there are some differences when considering NS AICs. The most remarkable feature is that several BH XRBs appear in region C, especially in model M4, too many ultra-luminous X-ray sources (ULXs) appear in this region, which destroys

the correlation badly. They all have relatively high speeds, typically  $\sim 150 - 300 \text{ km s}^{-1}$ . Additionally in the case of  $\alpha_{\text{CE}} = 0.2$  (i.e., models M8-M14), the  $L_X$  vs.  $R$  distribution still can not be well constructed. We suggest that precise velocity measurement of BH-XRBs are promising to discriminate different BH formation channels.

The evolution of  $L_X$  vs.  $R$  for model M1 is presented in Fig. 10. It can be seen that as the star formation proceeds, the  $L_X$  vs.  $R$  correlation is gradually built up till the time of about 20 Myr, then since the star formation quenches, the correlation disappears gradually as time goes on. So the  $L_X$

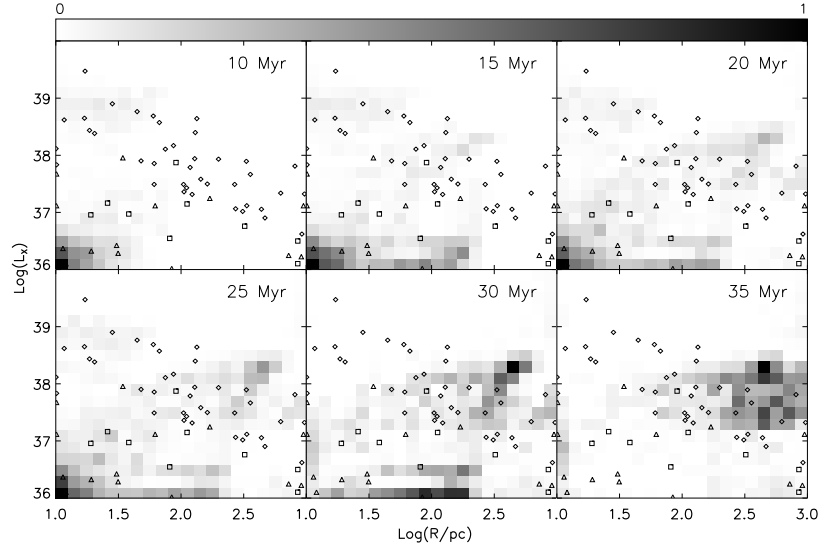


**Figure 10.** The evolution of the  $L_X - R$  distribution for model M1. The time is set at 10, 15, 20, 25, 30 and 35 Myr since the beginning of star formation, respectively.

vs.  $R$  correlation cannot hold all the time for individual cluster. In addition, we also examined the cases with/without Be-XRBs in the populations, and found that the impact of Be-XRB is minor over the whole evolution interested, due to its short transient characteristics.

Our modeled  $L_X$  vs.  $R$  correlation and its constraints on  $\alpha_{CE}$  is promising and sound, but they are still subject to some uncertainties and simplified treatments. Firstly, the binaries we evolved are all primordial ones, however they may also be produced by dynamical interactions, especially in dense star clusters. However in this formation channel, the massive stellar BHs which enter RLOF, thought as possible ULXs may have much longer evolution timescales (about several tens of Myr to  $\sim 100$  Myr since star formation, Mapelli et al. 2013, and see references therein), which is not likely the cases we studied here. Another simplified treatment is taken for the natal kicks. The role of natal kicks is essential for our studies, however little is yet known about either the amount of natal kicks or its distributions, especially for BH kicks (Brandt & Podsiadlowski 1995; Brandt, Podsiadlowski & Sigurdsson 1995; Gualandris et al. 2005; Fragos et al 2009, and references therein). It is reasonable to assume that BH receives a smaller natal kick in the absence of SN than in a SN scenario (Fryer & Kalogera 2001; Linden et al. 2010). However recent work by Repetto, Davies & Sigurdsson (2012) indicates that, in order to explain the observed distribution of LMXBs with BHs, natal kicks of BHs seem to be similar to that of NSs. The role of natal kicks, especially the amount and distribution of BH kicks deserves a thorough investigation, which will be presented in the forthcoming paper. Despite all of this, we note that our results are generally consistent with previous studies concerning the CE evolution. For example, a high value of  $\alpha_{CE}$  is required in order to account for the observed WDMS PCEBs (Davis et al. 2010), the shape of the delay-time distribution and the birth rate of SNe Ia for the double degenerate systems (Meng & Yang 2012), and HMXB XLFs (Zuo & Li

2014b), etc. Incorporating the kinematic evolution of HMXBs, we can give a more feasible-to-check observational properties of HMXBs, which may help understand the CE evolution and to constrain the value of  $\alpha_{CE}$ .

#### 4 SUMMARY

We have used a BPS code to model the luminosity versus displacement correlation of HMXBs in star-burst galaxies. We used the apparent correlation to constrain the CE parameter  $\alpha_{CE}$ , and find that within the framework of the standard energy formula for CE and core definition at mass  $X = 10\%$ , a high value of  $\alpha_{CE}$  around  $0.8 - 1.0$  is more preferable while  $\alpha_{CE} < \sim 0.4$  can not match the observation. We caution that alternative definitions for the core may change the value of  $\lambda$  by a factor of about two order of magnitude (for example, ‘entropy profile’ definition), which may translate directly the same uncertainty to the value of  $\alpha_{CE}$ . We split the  $L_X$  vs.  $R$  plane into three regions, named as regions A, B and C, specify the detailed properties of HMXB populations in each region. The results are listed in Tables 5-7, and summarized below.

(1) The high-luminosity ( $L_X > 10^{38}$  erg s $^{-1}$ ) sources in the  $10 < R < 100$  pc region are mainly BH-HeMS and NS-MS XRBs. They all have short orbital periods (several hours to  $\sim 1$  day). Their donor masses are around several solar masses to  $\sim 15 M_\odot$ . The system velocity is  $\sim 100 - 200$  km s $^{-1}$ .

(2) The low-luminosity ( $10^{36} < L_X < 10^{38}$  erg s $^{-1}$ ) sources in the  $10 < R < 100$  pc regions contain two species, i.e., high speed (peaks at  $\sim 200$  km s $^{-1}$ ) NS-XRBs with less massive ( $< \sim 10 M_\odot$ ) companions in short orbital periods (about days), and low speed ( $< \sim 30$  km s $^{-1}$ ) BH-XRBs powered by stellar winds from massive ( $\sim 30 - 60 M_\odot$ ) MS donors in wide orbits (periods about tens of days to even hundreds of days).

(3) The XRBs in the  $100 < R < 1000$  pc regions are mainly NS-XRBs. They mainly have relatively low-mass

( $< \sim 5 M_{\odot}$ ) companions. Their orbital periods are about several hours to days, and their system velocities are  $\sim 150$ – $300 \text{ km s}^{-1}$ .

Our studies show clearly that the CE parameter  $\alpha_{\text{CE}}$ , by governing the binary orbit during the CE, affects not only the outcome of the population, but also the kinematic motion, hence the spatial distribution of XRBs, revealing as distinct  $L_X$  vs.  $R$  distributions. So better measurements of  $L_X$  vs.  $R$  distribution, as well as the detailed properties of sources are promising to give a better constraint on the CE efficiency parameter. Our work motivates further high-resolution optical and X-ray observations of HMXB populations in nearby star-forming galaxies.

## ACKNOWLEDGEMENTS

This work was supported by the National Natural Science Foundation (grants 11103014 and 11003005), the Research Fund for the Doctoral Program of Higher Education of China (under grant number 20110201120034), the National Science Foundation of China (under grant number 10873008), the National Basic Research Program of China (973 Program 2009CB824800), the Fundamental Research Funds for the Central Universities and National High Performance Computing Center (Xi'an).

## REFERENCES

- Belczynski, K., Bulik, T., Fryer, C., Ruiter, A., Valsecchi, F., Vink, J. S., Hurley, J. R., 2010, *ApJ*, 714, 1217
- Belczynski, K., Dalogera A., Zezas A., Fabbiano, G., 2004a, *ApJ*, 601, L147
- Belczynski, K., Kalogera, V., Rasio, F. A., Taam, R. E., Zezas, A., Bulik, T., Maccarone, T. J., Ivanova, N., 2008, *ApJS*, 174, 223
- Belczynski, K., Wiktorowicz, G., Fryer, C. L., Holz, D. E., Kalogera, V., 2012, *ApJ*, 757, 91
- Belczynski, K., Ziolkowski, J., 2009, *ApJ*, 707, 870
- Bisschoux, B. 1998, M.Sc. Thesis, Univ. Amsterdam de Jager, C., Nieuwenhuijzen, H., & van der Hucht, K. A. 1988, *A&AS*, 72, 259
- Bondi, H., Hoyle, F., 1944, *MNRAS*, 104, 273
- Brandt N., Podsiadlowski Ph., 1995, *MNRAS*, 274, 461
- Brandt W. N., Podsiadlowski Ph., Sigurdsson S., 1995, *MNRAS*, 277, L35
- Chen, X., Han, Z., 2008, *MNRAS*, 387, 1416
- Chen, W., Shrader, C. R., Livio, M., 1997, *ApJ*, 491, 312
- Dai, H. L., Liu, X. W., Li, X. D., 2006, *ApJ*, 653, 1410
- Dalton, W. W., Sarazin, C. L., 1995, *ApJ*, 448, 369
- Davis, P. J., Kolb, U., Knigge, C., 2011, *MNRAS*, 1846
- Davis P. J., Kolb U., Knigge, C., 2012, *MNRAS*, 419, 287
- Davis P. J., Kolb U., Willems B., 2010, *MNRAS*, 403, 179
- De Marco O., Passy J., Moe M., Herwig F., Mac Low M., Paxton B., 2011, *MNRAS*, 411, 2277
- Dewi J.D.M., Tauris T.M., 2000, *A&A*, 360, 1043
- Dominik M., Belczynski K., Fryer C., Holz D., Berti E., Bulik T., Mandel I., O’Shaughnessy R., 2012, *ApJ*, 759, 52
- Eggleton, P. P. 1971, *MNRAS*, 151, 351
- Eggleton, P. P. 1972, *MNRAS*, 156, 361
- Eldridge J., Tout C., 2004a, *MNRAS*, 348, 201
- Eldridge J., Tout C., 2004b, *MNRAS*, 353, 87
- Fragos T., Willems B., Kalogera V., Ivanova N., Rockefeller G., Fryer C. L., Young P. A., 2009, *ApJ*, 697, 1057
- Fryer C. L., Belczynski K., Wiktorowicz G., Dominik M., Kalogera V., Holz D. E., 2012, *ApJ*, 749, 91
- Fryer C.L., Kalogera V., 2001, *ApJ*, 554, 548
- Fryer C. L., Rockefeller G., Warren M. S., 2006, *ApJ*, 643, 292
- Fryxell B., Olson K., Ricker P., Timmes F. X., Zingale M., Lamb D. Q., MacNeice P., Rosner R., Truran J. W., Tufo H., 2000, *ApJ Supp*, 131, 273
- Garcia M. R., Miller J. M., McClintock J. E., King A. R., Orosz J., 2003, *ApJ*, 591, 388
- Grimm H., Gilfanov M., Sunyaev R., 2003a, *MNRAS*, 339, 793
- Grimm H., Gilfanov M., Sunyaev R., 2003b, *Chin. J. Astron. Astrophys. Suppl.*, 3, 257
- Gualandris A., Colpi M., Portegies Zwart S., Possenti A., 2005, *ApJ*, 618, 845
- Han Z., 2008, *A&A*, 484, L31
- Han, Z., Podsiadlowski, P., & Eggleton, P. P. 1994, *MNRAS*, 270, 121
- Han Z., Podsiadlowski P., Eggleton P. P., 1995, *MNRAS*, 270, 121
- Han Z., Podsiadlowski P., Maxted P. F. L., Marsh T. R., 2003, *MNRAS*, 341, 669
- Han Z., Podsiadlowski P., Maxted P. F. L., Marsh T. R., Ivanova N., 2002, *MNRAS*, 336, 449
- Hjellming M.S., Webbink R.F., 1987, *ApJ*, 318, 794
- Ho L. C., Filippenko A. V., 1996a, *ApJ*, 466, L83
- Ho L. C., Filippenko A. V., 1996b, *ApJ*, 472, 600
- Hobbs G., Lorimer D. R., Lyne A. G., Kramer M., 2005, *MNRAS*, 360, 963
- Hurley J. R., Pols O. R., Tout C. A., 2000, *MNRAS*, 315, 543
- Hurley J. R., Tout C. A., Pols O. R., 2002, *MNRAS*, 329, 897
- Ivanova N., 2011, in Schmidtobreick L., Schreiber M. R., Tappert C., eds, *Proc. ASP Conf. Ser. 447, Evolution of Compact Binaries*. Astron. Soc. Pac., San Francisco, p. 91
- Ivanova N., Chaichenets S., 2011, *ApJL*, 731, 36
- Ivanova N. et al., 2013, *A&A Review*, 21, 591
- Kaaret P., Alonso-Herrero A., Gallagher J. S., Fabbiano G., Zezas A., Rieke M. J., 2004, *MNRAS*, 348, L28
- Kiel P.D., Hurley J.R., 2006, *MNRAS*, 369, 1152
- Kobulnicky H. A., Fryer C. L., 2007, *ApJ*, 670, 747
- Kroupa P., 2001, *MNRAS*, 322, 231
- Lasota J. P., 2001, *New Astronomy Reviews*, 45, 449
- Levine A., Rappaport S., Deeter J. E., Boynton P. E., Nagase F., 1993, *ApJ*, 410, 328
- Levine A., Rappaport S., Putney A., Corbet R., Nagase F., 1991, *ApJ*, 381, 101
- Linden T., Kalogera V., Sepinsky J. F., Prestwich A., Zezas A., Gallagher J., 2010, *ApJ*, 725, 19841
- Liu Q. Z., van Paradijs J., van den Heuvel E. P. J., 2005, *A&A*, 442, 1135
- Liu Q. Z., van Paradijs J., van den Heuvel E. P. J., 2006, *A&A*, 455, 1165
- Loveridge A. J., van der Sluys M. V., Kalogera V., *ApJ*, 2011, 743, 49
- Mapelli M., Ripamonti E., Zampieri L., Colpi M., 2011, *MNRAS*, 416, 1756
- Mapelli M., Zampieri L., Ripamonti E., Bressan A., 2013, *MNRAS*, 429, 2298
- Matteucci F., Tornambè A., 1987, *A&A*, 185, 51
- Maxted P. F. L., Napiwotzki R., Dobbie P. D., Burleigh M. R., 2006, *Nature*, 442, 543
- McSwain M. V., Gies D. R., 2005, *ApJS*, 161, 118
- Meng X., Yang W., 2012, *A&A*, 543, A137
- Mineo S., Gilfanov M., Sunyaev R., 2012, *MNRAS*, 419, 2095
- Morales-Rueda L., Maxted P. F. L., Marsh T. R., North R. C., Heber U., 2003, *MNRAS*, 338, 752
- Nelemans G., Tout C. A., 2005, *MNRAS*, 356, 753
- Nelemans G., Verbunt F., Yungelson L. R., Portegies Zwart S. F., 2000, *A&A*, 360, 1011
- O’Shea, B. W., Nagamine, K., Springel, V., Hernquist, L., Norman, M. L. 2005, *ApJ Supp*, 160, 1
- Paczynski P., 1976, in Eggleton P., Mitton S., Whelan J., eds, *Proc. IAU Symp. 73, Structure and Evolution of Close Binary Systems*, p. 75
- Paczynski B., 1990, *ApJ*, 348, 485
- Passy J.-C., De Marco O., Fryer C. L., Herwig F., Diehl S., Oishi J. S., Mac Low M.-M., Bryan G. L., Rockefeller G., 2012, *ApJ*, 744, 52
- Podsiadlowski P., Langer N., Poelarends A. J. T., Rappaport S., Heger A., Pfahl E., 2004, *ApJ*, 612, 1044
- Podsiadlowski P., Rappaport S., Pfahl E. D., 2002, *ApJ*, 565, 1107
- Podsiadlowski P., Rappaport S. A., Han Z., 2003, *MNRAS*, 341, 385
- Politano M., Weiler M., 2006, *ApJ*, 641, L1373
- Politano M., Weiler M., 2007, *ApJ*, 665, 663
- Raguzova N. V., Popov S. B., 2005, *Astron. Astrophys. Trans.*, 24, 151
- Rappaport S. A., Podsiadlowski P., Pfahl E., 2005, *MNRAS*, 356, 401
- Rasio F., Livio M., 1996, *ApJ*, 471, 366
- Reig P., 2011, *Ap&SS*, 332, 1
- Repetto S., Davies M. B., Sigurdsson S., 2012, *MNRAS*, 425, 2799
- Repolust T., Puls J., Herrero A., 2004, *A&A*, 415, 349
- Ricker P. M., Taam R. E., 2008, *ApJ*, 672, L41
- Ricker P. M., Taam R. E., 2012, *ApJ*, 746, 74
- Sana H. et al., 2013, *A&A*, 550, 107
- Sandquist E. L., Taam R. E., Burkert A., 2000, *ApJ*, 533, 984
- Sandquist E. L., Taam R. E., Chen X., Bodenheimer P., Burkert A., 1998, *ApJ*, 500, 909
- Shao Y., Li, X., 2014, in preparation
- Slettebak A., 1988, *PASP*, 100, 770
- Smith L. J., Gallagher J. S., 2001, *MNRAS*, 326, 1027
- Soker N., 2004, *New Astron.*, 9, 399
- Sternberg A., 1998 *ApJ*, 506, 721
- Taam R. E., Ricker P. M., 2010, *New Astronomy Reviews*, 54, 65
- Tauris T.M., Dewi J.D.M., 2001, *A&A*, 369, 170
- Tutukov A. V., Yungelson L. R., 1979, in *Mass Loss and Evolution of O-Type Stars*, ed. P. S. Conti & W. H. de Loore ( Dordrecht: Reidel), 216
- van Kerkwijk M. H. et al., 1992, *Nature*, 355, 703

- van der Sluys M. V., Verbunt F., Pols O. R., 2006, *A&A*, 460, 209
- Vink J. S., de Koter A., Lamers H. J. G. L. M., 2001, *A&A*, 369, 574
- Webbink R. F., 1984, *ApJ*, 277, 355
- Webbink R. F., 1988, in *The Symbiotic Phenomenon*, ed. J. Mikolajewska, M. Friedjung, S. J. Kenyon & R. Viotti (Kluwer: Dordrecht), p.311
- Webbink R. F., 2008, in *Astrophysics and Space Science Library*, Vol. 352, "Short-Period Binary Stars: Observations, Analyses, and Results", ed. E. F. Milone, D. A. Leahy, D. W. Hobill, 233
- Weisskopf M.C., Tananbaum H.D., Van Speybroeck L.P., O'Dell S.L., 2000. *Proc. SPIE*, 4012, 2
- Xu X. J., Li X. D., 2010, *ApJ*, 716, 114
- Ziolkowski J., 2002, *MmSAI*, 73, 1038
- Zorotovic M., Schreiber M. R., Gänsicke B. T., Nebot Gómez-Morán A., 2010, *A&A*, 520, 86
- Zuo Z. Y., Li X. D., Gu Q. S., 2014a, *MNRAS*, 437, 1187
- Zuo Z. Y., Li X. D., Liu X. W., 2008, *MNRAS*, 387, 121
- Zuo Z. Y., Li X. D., 2010, *MNRAS*, 405, 2768
- Zuo Z. Y., Li X. D., 2011, *ApJ*, 733, 5
- Zuo Z. Y., Li X. D., 2014b, preprint (astro-ph/1310.6535)